Enhancement of visible light photocatalytic pharmaceutical degradation and hydrogen evolution of Bi_5O_7Br by in situ disorder engineering

Fang-xia XIE[1,2], Lu-lu ZHANG[2], Xiao ZHANG[1], Mei ZHANG[2],

Xuan JIAN[3], Jian-xin LIU[2], Xiao-chao ZHANG[2], Ya-wen WANG[2], Rui LI[1,2], Cai-mei FAN[1,2]

1. College of Environmental Science and Engineering, Taiyuan University of Technology, Taiyuan 030024, China;
2. College of Chemical Engineering and Technology, Taiyuan University of Technology, Taiyuan 030024, China;
3. Shaanxi Key Laboratory of Chemical Reaction Engineering, College of Chemistry and Chemical Engineering, Yan'an University, Yan'an 716000, China

Abstract: In order to simultaneously solve the problems of the poor light absorption capacity and high recombination rate of photogenerated carriers, Bi_5O_7Br photocatalyst with abundant ordered/disordered structures (O/D-Bi_5O_7Br) was prepared through a simple in situ disorder engineering. The prepared samples were characterized by XRD, TEM, HRTEM, SAED, XPS, UV-Vis diffuse reflectance spectra (DRS), and the activity was evaluated by photocatalytic degradation of tetracycline hydrochloride (TC) and hydrogen evolution under visible light irradiation. Results revealed that the ordered/disordered structure not only enhances the light absorption ability, uplifts conduction band position, facilitates the transfer and separation of photogenerated carriers, but also offers abundant unsaturated atoms as active sites for the photocatalytic process. Therefore, O/D-Bi_5O_7Br exhibits a high hydrogen evolution rate of 38.12 μmol/(g·h) and superior TC degradation rate of 86% within 135 min.

Key words: Bi_5O_7Br; disordered engineering; pharmaceutical degradation; hydrogen evolution; visible light

1 Introduction

Over the past generation, the human race has been faced with significant challenges because of the increasing severity of environmental pollution and the gradual decline of fossil energy [1−3]. As for environmental pollution, pharmaceuticals have been frequently detected in various water resources worldwide. In particular, tetracycline hydrochloride (TC), the second most common antibiotic, has been extensively applied to treating infectious diseases in humans and animals, thus resulting in the presence of trace residues in the environment that trigger the development of antibiotic pathogens and continue to threaten human health [4,5]. Thus, the

development of efficient and cost-effective treatment technologies to degrade harmful pharmaceuticals has extremely significant meaning in enhancing our future welfare and civilization [6,7]. Over the last few years, semiconductor photocatalysis technology, as the most promising method for environmental remediation and solar energy conversion, has been intensively investigated [8−12]. Many catalysts have been applied to pharmaceutical degradation, such as metal-organic frameworks (MOF), metal oxide, sulfide, graphitic carbon nitride, and bismuth based materials. However, these materials commonly suffer from low light absorption capacity and the rapid recombination of photoproduction carriers. Hence, efficient, clean, and economic catalysts should be explored to enhance the degradation of

photocatalytic pharmaceuticals.

In recent years, nonstoichiometric bismuth halide photocatalysts ($Bi_xO_yBr_z$) have been studied [13]. Their open-layered crystalline structure can produce an internal static electric field, eventually inhibiting the recombination of photogenerated electron−hole pairs effectively. In addition, the bandgap structure of $Bi_xO_yBr_z$ can be regulated by releasing the amount of Br^-, so as to obtain a suitable band structure for visible light-responsive ability. Therefore, $Bi_xO_yBr_z$ has been widely studied as photocatalyst for photocatalytic pharmaceuticals degradation, and some remarkable achievements have been made [14,15]. However, among the large family of $Bi_xO_yBr_z$, Bi_5O_7Br has rarely been discussed despite having the strongest electron reduction ability and higher photostability [16]. This gap is mainly due to its relatively rapid recombination of photogenerated carriers and large bandgap, which absorbs UV light only. Thus, Bi_5O_7Br photocatalyst should be modified to improve its photocatalytic activity.

Recent studies have shown that solid structure materials can be subdivided into three forms: amorphous, quasi-crystalline, and crystalline. Notably, amorphous materials have distinctive short-range ordered but long-range disordered atomic arrangements, which give them distinct electronic, mechanical, magnetic, and optical properties relative to crystals and quasi-crystals materials with long-range atomic order. The most remarkable advantage of amorphous materials is their much smaller bandgap than that of their crystalline counterparts. This unique quality allows that amorphous materials have a wider light absorption range [17]. Meanwhile, the disordered structure in amorphous materials could act as electron capture sites, which could inhibit the recombination efficiency of photogenerated electron−hole pairs and thus delay the lifespan of active species [18]. As for Bi-based compounds, the existence of disorder can cause the displacement of Bi^{3+} and O^- from their ideal positions due to the stereochemically active $6s^2$ electron lone pair on Bi^{3+} and then offer abundant unsaturated atoms as active sites for the photocatalytic process [19−21]. In addition, in situ disorder engineering can supply barrier-free tight contact and accelerate the charge transfer efficiently [22]. Thus, in situ constructing Bi_5O_7Br photocatalyst with abundant ordered/ disordered structures through disorder engineering might be a suitable model for enhancing visible light photocatalytic pharmaceutical degradation and extending the application scope of Bi_5O_7Br. However, no relevant report has focused on the disordered engineering regulation of $Bi_xO_yBr_z$ to promote its photocatalytic activity.

Herein, we put forward a facile disorder engineering for the in situ synthesis of Bi_5O_7Br with abundant ordered/disordered structures and investigate the photocatalytic activities for pharmaceutical degradation and hydrogen evolution. The key step of this new technique is to mix $Bi(NO_3)_3·5H_2O$ and $NaBrO_3$, and then adjust the pH by $NH_3·H_2O$. Although the reaction process is simple, it is very effective in the in situ formation of Bi_5O_7Br with abundant ordered/disordered structures.

2 Experimental

2.1 Materials

In this work, sodium bromate ($NaBrO_3$) was obtained from Guangfu Fine Chemical Research Institute, Tianjin, China. Bismuth nitrate penta-hydrate ($Bi(NO_3)_3·5H_2O$) was purchased from the Sinopharm Chemical Reagent Co., Ltd., Shanghai, China. Ammonia hydroxide ($NH_3·H_2O$), ethanol absolute (CH_3CH_2OH) and methanol (CH_3OH) were produced by Kermel Chemical Reagent Co., Ltd., Tianjin, China. Chloroplatinic acid ($H_2PtCl_6·6H_2O$) and tetracycline hydrochloride (TC) were provided with Aladdin Reagent Co., Ltd. All these chemicals were analytical reagent (AR) grades that can be used directly.

2.2 Preparation of photocatalysts

A facile in situ disorder engineering was used to prepare the photocatalyst. The concrete steps are as follows: exactly 4.85 g of $Bi(NO_3)_3·5H_2O$ was dispersed into 50 mL of distilled water with continuous stirring. Meanwhile, 1.51 g of $NaBrO_3$ was dissolved into 40 mL of distilled water and then added into the $Bi(NO_3)_3·5H_2O$ solution with vigorous stirring for 0.5 h. Then, 2.5 mL of $NH_3·H_2O$ was used to adjust the pH and continually facilitate the reaction at 20 °C for 3 h. Finally, the sample was collected and washed several times with distilled water and ethanol to remove residual species and then dried at 60 °C for more than 6 h.

The Bi_5O_7Br with abundant ordered/disordered structures was obtained and called O/D-Bi_5O_7Br. For comparison and analysis, the ordered Bi_5O_7Br and disordered Bi_5O_7Br were obtained by the same process at 35 and 0 °C, and named O-Bi_5O_7Br and D-Bi_5O_7Br, respectively.

2.3 Characterization

X-ray diffraction (XRD) patterns were recorded on a Rigaku D/max 2700 diffractometer operated at 30 mA and 40 kV with Cu K$_\alpha$ (λ=1.5418 Å) radiation and the 2θ ranging from 10º to 70º. X-ray photoemission spectroscopy (XPS) and valence band (VB)-XPS with an Mg K$_\alpha$ X-ray source operating at 20 kV were carried out with VG MultiLab 2000 system and the binding energy of samples was calibrated by using the signal for carbon (284.65 eV for C 1s) as a reference. The transmission electron microscopy (TEM), high-resolution transmission electron microscopy (HRTEM) images and selected area electron diffraction (SAED) patterns were collected on a JEOL−2011 device at an accelerating voltage of 200 kV. UV-Vis diffuse reflectance spectra (UV-Vis DRS) were carried out by using an UV−2450 spectrophotometer with $BaSO_4$ sample as a reference. Steady-state photoluminescence (PL) spectra were recorded by using an Edinburgh instrument FLS980 series of fluorescence spectrometers.

2.4 Photocatalytic activity

The activity of the photocatalysts was evaluated by degrading TC under visible light irradiation. Typically, 50 mg of the sample was dispersed into 100 mL of the TC solution (10 mg/L). After reaching adsorption−desorption equilibrium in the dark for 20 min, the suspension was placed in visible light. At 15 min intervals, a certain amount of suspension was taken out, centrifuged (800 r/min, 5 min), and further analyzed using a Varian Cary 50 UV-Vis spectrophotometer. Furthermore, the photocatalytic activity of water splitting hydrogen evolution was also tested to verify that disorder engineering could extend the application scope of Bi_5O_7Br. Specifically, the catalyst (0.1 g) was added in deionized water (80 mL, 40 vol.% CH_3OH), and the co-catalyst Pt (1 wt.%) was loaded on the surfaces of the samples by the in situ photo-deposition with H_2PtCl_6. Then, the system was purged with high purity argon for 20 min to remove

the air completely and irradiated under a Xe lamp (300 W) equipped with a 420 nm cut-off filter (Perfect Light, China). In this process, the temperature of the system was maintained at 5 °C with a cooling cycle device. Finally, the amount of hydrogen generation was quantitatively analyzed in a specific time interval through online gas chromatography (GC9700).

2.5 Photoelectrochemical measurements

Electrochemical impedance spectroscopy (EIS), photocurrent and Mott−Schottky tests were carried out on a CHI−660E electrochemical workstation using a three-electrode system (Shanghai Chenhua, China). The samples spread on indium tin oxide, Ag/AgCl electrode, and Pt mesh served as the working electrodes, reference electrodes, and counter electrodes, respectively. The light was produced using a 300 W Xe lamp equipped with a 420 nm cutoff filter.

3 Results and discussion

3.1 Characterization of photocatalysts

The crystal and phase structures of the as-synthesized samples were characterized by XRD analysis. As shown in Fig. 1, the detectable peaks of the obtained O-Bi_5O_7Br samples at 35 °C correspond well to those of Bi_5O_7Br (PDF#97-024-1125). The presence of sharp peaks indicates that this material possesses long-range order, which proves the successful synthesis of ordered Bi_5O_7Br material. Meanwhile, the samples only show a broad reflection at 2θ of 28.3° as the temperature falls to 0 °C, indicating the successful synthesis of
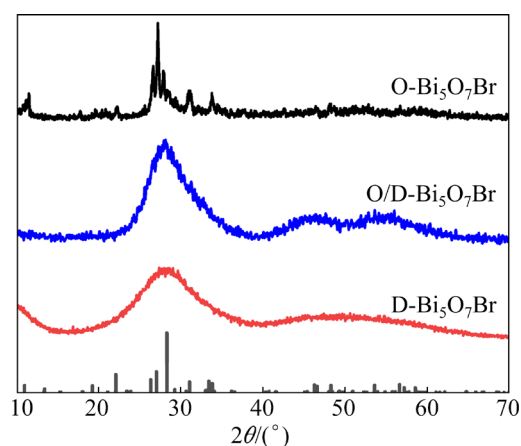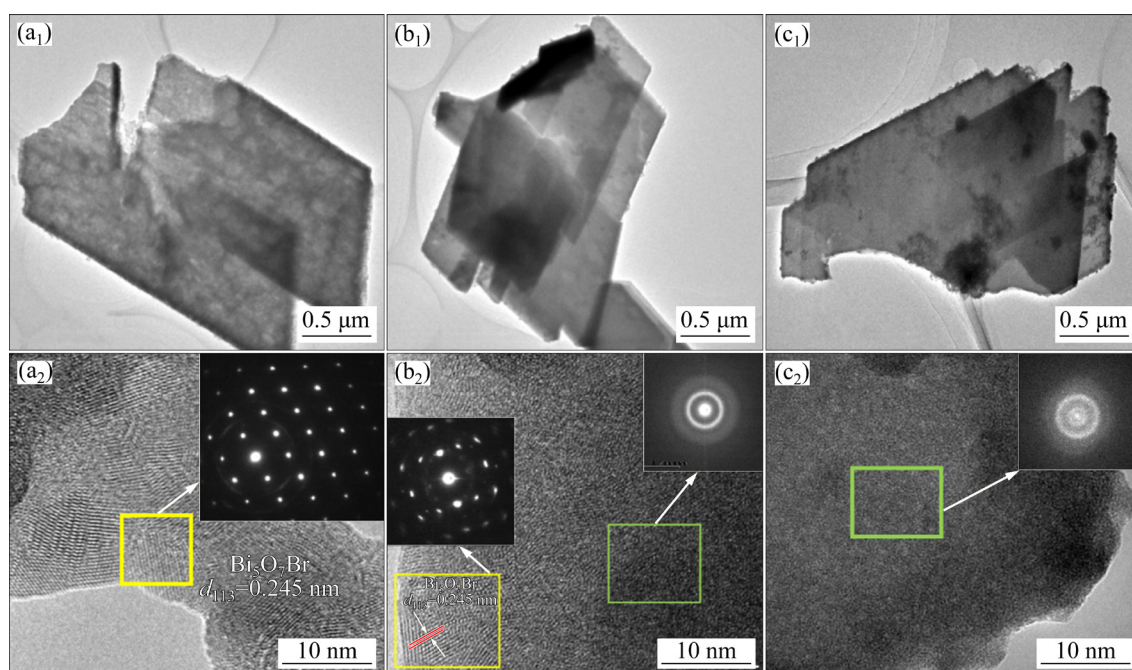

Fig. 1 XRD patterns of O-Bi_5O_7Br, O/D-Bi_5O_7Br and D-Bi_5O_7Br

the pure disordered Bi_5O_7Br material (D-Bi_5O_7Br). In particular, when the reaction temperature of changes to 20 °C for O/D-Bi_5O_7Br, two broad humps ranging from 45° to 55° (peak positions at 46.5° and 53.7°) and a relatively strong and broad characteristic peak (28.3°) are observed (Fig. 1), which suggests that its crystallinity is worse than that of O-Bi_5O_7Br. This phenomenon is attributed to the amorphous Bi_5O_7Br and indicates that the synthesized O/D-Bi_5O_7Br sample is composed of ordered/disordered structures [23,24].

To verify the conclusion, TEM and HRTEM were performed to further characterize the samples. As shown in Figs. 2(a_1, b_1, c_1), O-Bi_5O_7Br, O/D-Bi_5O_7Br and D-Bi_5O_7Br have the stacking of nanosheets with a size of ~400 nm. Furthermore, HRTEM images and SAED patterns offer an intuitive observation of the samples' crystalline microstructure. In the HRTEM image and SAED pattern of O-Bi_5O_7Br (Fig. 2(a_2)), clear lattice fringes and no internal defects are shown, suggesting its high crystallinity. The lattice spacing (d) is measured to be 0.245 nm, which corresponds well to the (113) plane of Bi_5O_7Br. Moreover, the regular and periodic arrangement of diffraction spots in the SAED diagram of O-Bi_5O_7Br further confirms its ordered structures. By contrast, the HRTEM images of D-Bi_5O_7Br show disordered regions without clear lattice fringes, and the SAED

patterns exhibit a closed diffraction ring, which is indicative of its disordered structure (Fig. 2(c_2)). For O/D-Bi_5O_7Br (Fig. 2(b_2)), the HRTEM images show disordered regions (green area) and ordered regions (yellow area). Furthermore, the SAED pattern in the green area exhibits a closed diffraction ring, and the SAED pattern in the yellow area shows a fringe with a lattice spacing of 0.245 nm corresponding to the (113) plane of Bi_5O_7Br. The result indicates that the disordered structure has been introduced into the ordered catalyst and demonstrates that the basic lattice structure of Bi_5O_7Br has not been destroyed [25−27]. This phenomenon further strongly proves the successful synthesis of O/D-Bi_5O_7Br with abundant ordered/ disordered structures.

The element compositions and valence states of the samples were characterized by XPS in detail. As shown in Fig. 3(a), the full-scale XPS spectrum reveals the existence of Bi, Br, O, and C elements. The Bi 4f and Br 3d XPS spectra of O-Bi_5O_7Br, O/D-Bi_5O_7Br, and D-Bi_5O_7Br are almost identical, indicating the similar bonding environments of Bi and Br atoms before and after disordered engineering regulation. In the Bi 4f spectra of O-Bi_5O_7Br, O/D-Bi_5O_7Br, and D-Bi_5O_7Br (Fig. 3(b)), two peaks at binding energies of 164.28, 164.24, and 164.29 eV; and 158.97, 158.93, and 159.02 eV can be respectively attributed to Bi $4f_{5/2}$ and Bi $4f_{7/2}$,

Fig. 2 TEM, HRTEM images and SAED patterns (in insets) of O-Bi_5O_7Br (a_1, a_2), O/D-Bi_5O_7Br (b_1, b_2), and D-Bi_5O_7Br (c_1, c_2)
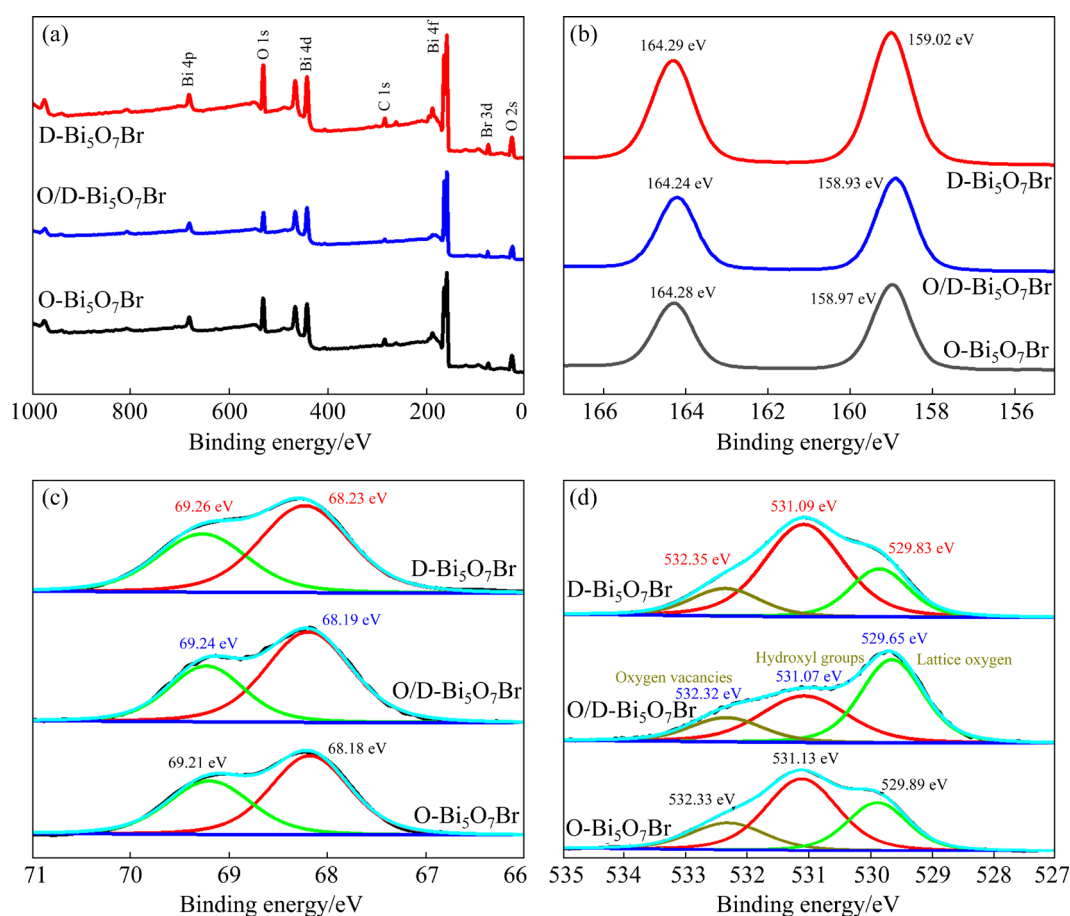
Fig. 3 XPS spectra of O-Bi$_5$O$_7$Br, O/D-Bi$_5$O$_7$Br and D-Bi$_5$O$_7$Br: (a) Survey; (b) Bi 4f; (c) Br 3d; (d) O 1s

which are characteristics of Bi^{3+} in the samples [28,29]. In addition, the Br 3d high- resolution XPS spectrum (Fig. 3(c)) showing two peaks at 69.21, 69.24, and 69.26 eV; and 68.18, 68.19, and 68.23 eV can be respectively attributed to Br 3d$_{3/2}$ and Br 3d$_{5/2}$, which indicates the presence of bromide ions in the O-Bi$_5$O$_7$Br, O/D-Bi$_5$O$_7$Br, and D-Bi$_5$O$_7$Br [30]. The O 1s spectra of the O-Bi$_5$O$_7$Br, O/D-Bi$_5$O$_7$Br, and D-Bi$_5$O$_7$Br samples show obvious differences. The peaks at binding energies of 529.89, 529.65, and 529.83 eV originate from the lattice oxygen, thus suggesting the existence of a bismuth-oxygen bond [31]. Meanwhile, the peaks at binding energies of 531.13, 531.07, and 531.09 eV are ascribed to chemisorbed H$_2$O or OH$^-$ on the sample surface [32]. Besides, the peaks located at binding energies of 532.33, 532.32, and 532.35 eV can be indexed to the oxygen atoms near the oxygen vacancies [33,34] (Fig. 3(d)). The comparison reveals the changes in the peaks and concentrations of surface lattice oxygen species. This phenomenon can indirectly demonstrate the formation of defects in disorder

engineering, which can act as active sites for photocatalytic reaction [35,36]. Based on the above results, we verify the successful preparation of Bi$_5$O$_7$Br with an abundant ordered/disordered structure.

3.2 Photocatalytic activity

Given the attractive ordered/disordered characteristic of O/D-Bi$_5$O$_7$Br, it is expected to be a competent catalyst for photocatalytic reaction. Herein, the photocatalytic degradation of TC is carried out to investigate the photocatalytic performance of O/D-Bi$_5$O$_7$Br under visible light (Fig. 4(a)). The results show that the TC cannot be degraded without a photocatalyst, and that O/D-Bi$_5$O$_7$Br shows good activity with 86% TC degradation rate after 135 min of visible light irradiation; such a rate is 25% and 32% higher than those of O-Bi$_5$O$_7$Br and D-Bi$_5$O$_7$Br, respectively. Furthermore, the degradation activity has a slight change during the four experiment cycles, confirming the superior stability of O/D-Bi$_5$O$_7$Br (Fig. 4(b)).
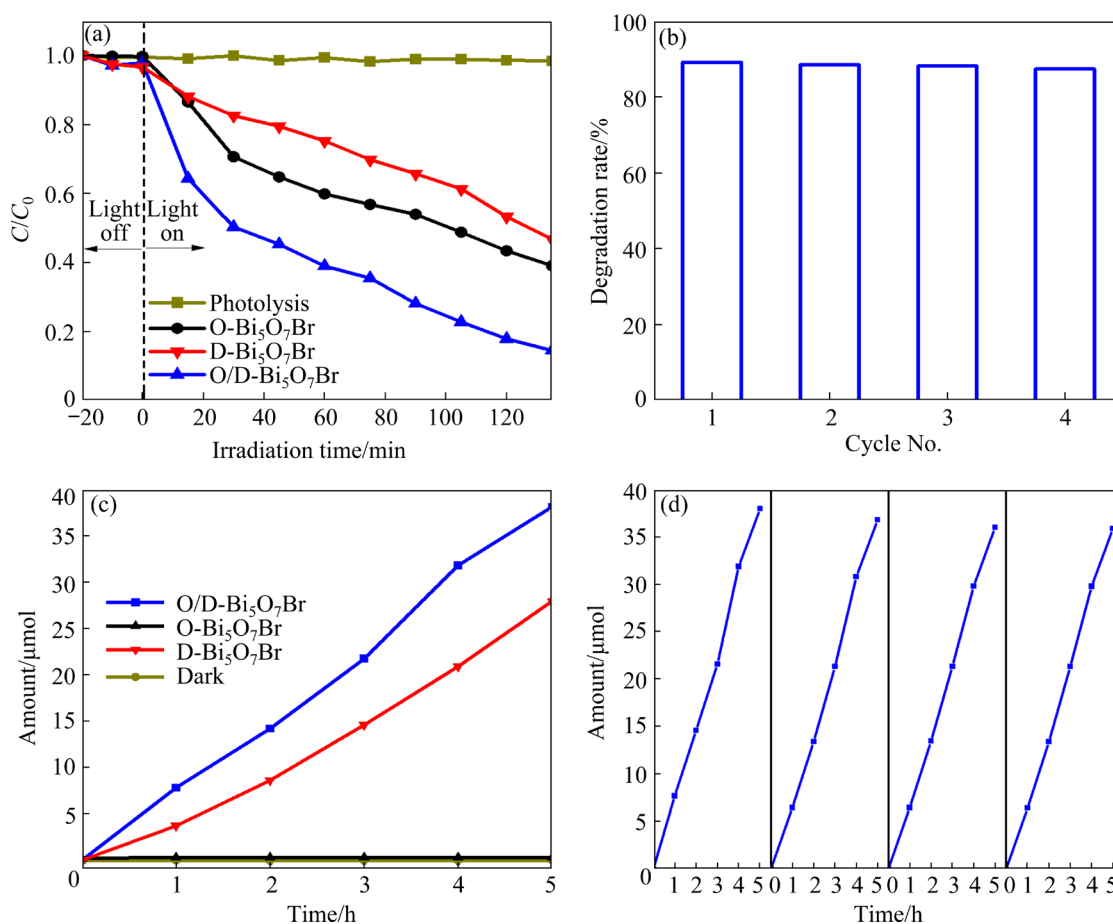
Fig. 4 Photocatalytic activity under visible light irradiation: (a) TC degradation (C is remaining TC concentration at time t; C_0 is intitial TC concentration); (b) Recycling experiment results of TC degradation for O/D-Bi$_5$O$_7$Br; (c) Photocatalytic hydrogen evolution experiment results; (d) Recycling experiment results of hydrogen evolution for O/D-Bi$_5$O$_7$Br

To verify whether disorder engineering could extend the application scope of Bi$_5$O$_7$Br, the photocatalytic hydrogen evolution activity of the prepared samples was also evaluated. The hydrogen evolution results of the samples from water under visible light irradiation are shown in Fig. 4(c). No hydrogen is detected for O-Bi$_5$O$_7$Br, but the amount of hydrogen is enhanced gradually over time in the presence of O/D-Bi$_5$O$_7$Br, and O/D-Bi$_5$O$_7$Br exhibits a high hydrogen evolution rate of about 38.12 μmol/(g·h). Furthermore, O/D-Bi$_5$O$_7$Br shows a relatively small change in hydrogen evolution rate after four cycles (Fig. 4(d)), thus suggesting the favorable stability of the structure. These results indicate that O/D-Bi$_5$O$_7$Br with abundant ordered/disordered structures plays an essential role in improving photocatalytic activity [37].

3.3 Photoelectrochemical performance

To explore the optical excitation processes in the special ordered/disordered structure, we conducted photoelectrochemical measurements. PL spectra were obtained to understand the recombination efficiency of electrons and holes under ambient conditions (Fig. 5(a)). O/D-Bi$_5$O$_7$Br displays the lowest emission peak at 413 nm and exhibits a light red-shift because of the alteration in its internal structure; such property ensures that the ordered/disordered structures can restrain the electron−hole recombination efficiently. Furthermore, photocurrent measurement was conducted to study the separation and transfer of the photoinduced charge carriers of the samples (Fig. 5(b)). O/D-Bi$_5$O$_7$Br clearly exhibits a higher current density than D-Bi$_5$O$_7$Br and O-Bi$_5$O$_7$Br because of the special ordered/disordered structures. Such property benefits the separation and transfer of photo-generated holes and electrons and helps prolong the lifetime of photogenerated charge carriers so that more electrons can participate in the photocatalytic reaction, which correspond to the result of the photocatalytic activity [38]. EIS measurement was
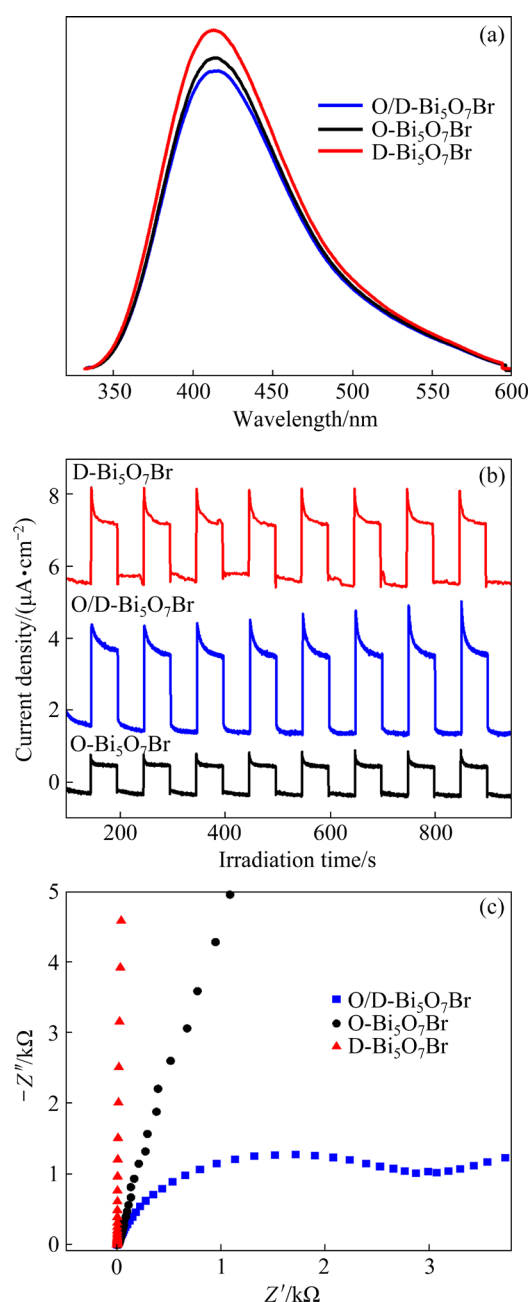
Fig. 5 Steady-state photoluminescence spectra (a), transient photocurrent response (b) and electrochemical impedance spectra (c) of O-Bi$_5$O$_7$Br, O/D-Bi$_5$O$_7$Br and D-Bi$_5$O$_7$Br

performed to investigate the interfacial transfer efficiency behaviors of the carriers (Fig. 5(c)). The radius of the Nyquist plots shows the feature of the charge transfer process of the samples. The radius of the curve of O/D-Bi$_5$O$_7$Br is significantly smaller than those of D-Bi$_5$O$_7$Br and O-Bi$_5$O$_7$Br, indicating the lower charge transfer resistance, which means that the recombination rate of the electron−hole pair is also low [16]. As discussed herein, O/D-Bi$_5$O$_7$Br with abundant ordered/disordered structures was

proved to facilitate the separation of the electrons and holes, thereby making more electrons participate in the reaction.

3.4 Photocatalytic mechanism

UV-Vis DRS was measured to study the optical properties of the samples (Fig. 6(a)). The as-prepared O-Bi$_5$O$_7$Br, O/D-Bi$_5$O$_7$Br, and D-Bi$_5$O$_7$Br display absorption edges of about 410, 428, and 413 nm, respectively. According to the Kubleka−Munk equation of $\alpha h\nu = A(h\nu - E_g)^{1/2}$, where α, $h\nu$, A, and E_g are the absorption coefficient, light frequency, constant, and bandgap energy, respectively [39], the bandgaps of O-Bi$_5$O$_7$Br, O/D-Bi$_5$O$_7$Br, and D-Bi$_5$O$_7$Br are estimated to be 2.83, 2.73, and 2.81 eV, respectively (the inset of Fig. 6(a)). Compared with O-Bi$_5$O$_7$Br and D-Bi$_5$O$_7$Br, O/D-Bi$_5$O$_7$Br has a narrower band edge, which may be due to the presence of an ordered/ disordered structure. To analyze the band structure of the samples, we employed the valence band XPS spectrum (VB-XPS) combined with the Mott−Schottky plot. Firstly, VB-XPS was used to measure the energy gap (E_{vf}) between the valance band potential (E_{VB}) and Fermi level (E_f) [40]. Figure 6(b) indicates that the E_{vf} values of O-Bi$_5$O$_7$Br and O/D-Bi$_5$O$_7$Br are 2.16 and 1.47 eV, respectively. Secondly, the Mott−Schottky plot is used to obtain the types of semiconductors and flat band potentials (E_{FB}) [41]. As shown in Fig. 6(c), the E_{FB} values of O-Bi$_5$O$_7$Br and O/D-Bi$_5$O$_7$Br are respectively calculated to be 0.25 and 0.60 V (vs Ag/AgCl), which correspond to 0.47 and 0.82 V (vs NHE), respectively [42]. The positive slopes of $1/C_1^2$ (C_1 is the capacitance of space charge layers) versus potential exhibit the n-type semiconductor characteristics of O-Bi$_5$O$_7$Br and O/D-Bi$_5$O$_7$Br, where E_f is equal to E_{FB} [40], thus, the E_f values of O-Bi$_5$O$_7$Br and O/D-Bi$_5$O$_7$Br are 0.47 and 0.82 V, respectively. Therefore, according to the equation of $E_{VB} = E_{vf} + E_{FB}$, the VB positions of O-Bi$_5$O$_7$Br and O/D-Bi$_5$O$_7$Br are estimated to be 2.63 and 2.29 V, respectively. From the equation $E_{CB} = E_{VB} - E_g$, the CB positions of O-Bi$_5$O$_7$Br and O/D=Bi$_5$O$_7$Br are estimated to be −0.20 and −0.44 V, respectively. The results show that the ordered/disordered structures can broaden the visible light response range and uplift the CB position, making the electrons have stronger reduction ability. In addition, these results correspond to those of the
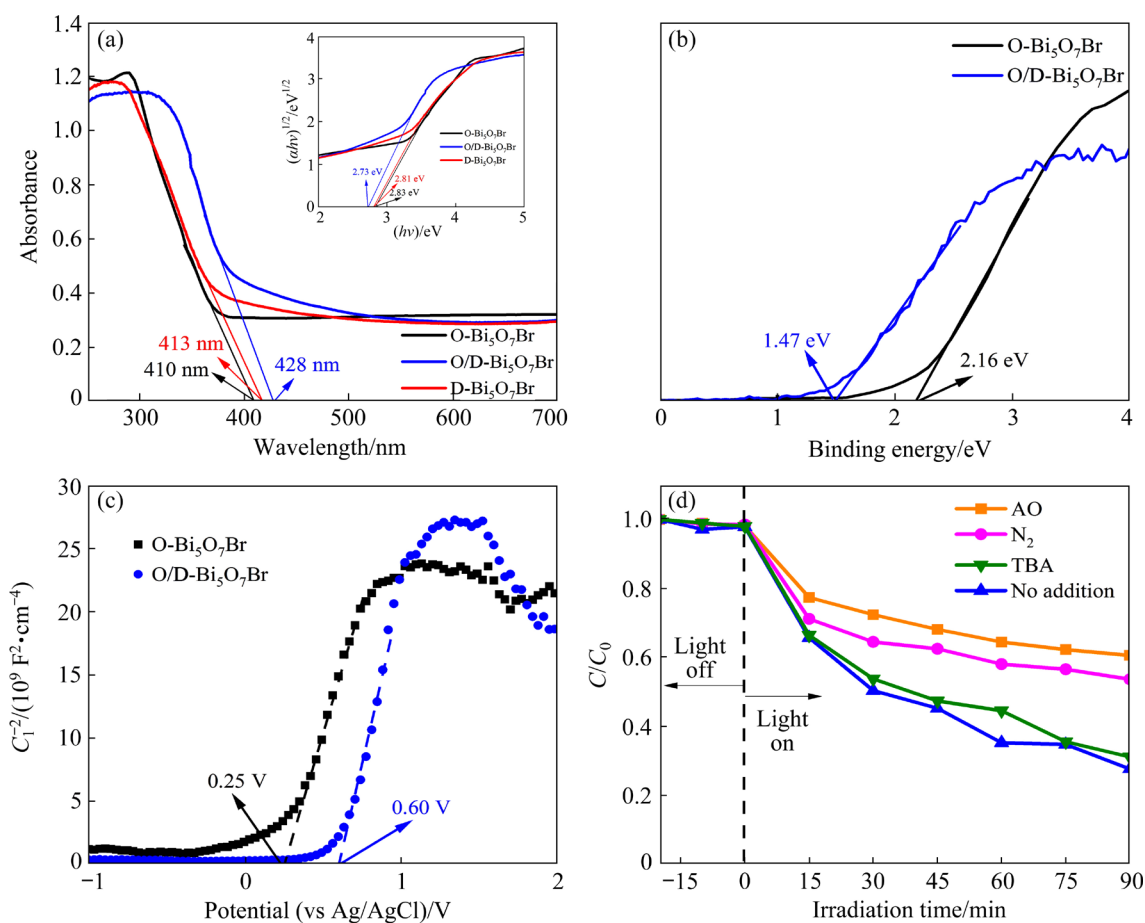
Fig. 6 (a) UV-Vis DRS of samples (the inset is plots of $(ahv)^{1/2}$ versus energy (hv)); (b) VB-XPS spectra of O-Bi_5O_7Br and O/D-Bi_5O_7Br; (c) Mott−Schottky curves of O-Bi_5O_7Br and O/D-Bi_5O_7Br, respectively; (d) Scavenging experiment results of O/D-Bi_5O_7Br

photocatalytic hydrogen evolution activity. Thirdly, N_2 purging, tertiary butanol (TBA), and ammonium oxalate (AO) were respectively used to capture the active species of $\cdot O_2^-$, $\cdot OH$, and holes (h^+) in the TC photocatalytic degradation process over the O/D-Bi_5O_7Br samples under visible light irradiation. As seen in Fig. 6(d), the TC degradation rate does not decrease when TBA is added, indicating that $\cdot OH$ radicals have no effect on the O/D-Bi_5O_7Br photocatalysis reaction system. After adding AO or N_2 to the reaction solution, the TC photocatalytic degradation rate drops, showing that h^+ and $\cdot O_2^-$ are the main active species. Moreover, h^+ has a more significant impact than O_2^- in this process.

These results reveal that the satisfactory photocatalytic TC degradation and hydrogen evolution activities of O/D-Bi_5O_7Br are attributable to their special physicochemical structure. The band structure and schematic representation of the photocatalytic reaction of O/D-Bi_5O_7Br are depicted

in Fig. 7. As for the photocatalytic degradation reaction, under the irradiation of visible light, the electrons (e) are excited to the CB potential position (−0.44 V) from the VB of O/D-Bi_5O_7Br (2.29 V). Then, the excited electrons are trapped by O_2 molecules, and $\cdot O_2^-$ radicals are produced on the basis of the less redox potential (−0.046 eV) of $O_2/\cdot O_2^-$. The holes left in VB of O/D-Bi_5O_7Br and $\cdot O_2^-$ photodegrade the organic compounds. As for the photocatalytic hydrogen evolution reaction, the excited electrons participate in hydrogen evolution and the holes are quickly consumed by the sacrificial agents. The ordered/disordered structures clearly play a key role in the photocatalytic degradation and hydrogen evolution reaction. Firstly, the solar absorption ability is enhanced by introducing disordered structure, leading to the increase in visible absorption ability and photoinduced carriers of Bi_5O_7Br. Secondly, the ordered/disordered structures act as electron scavengers, suppressing the recombination of

electrons and holes and promoting electron migration towards the surface for further reaction. Thirdly, the ordered/disordered structures also offer abundant unsaturated atoms as active sites for the photocatalytic process. Moreover, the photogenerated electrons have strong reduction ability because of the more negative CB position, which results in the full and efficient use of photogenerated electrons. As a result, Bi_5O_7Br with abundant ordered-disordered structures shows efficient TC degradation and hydrogen evolution performance.
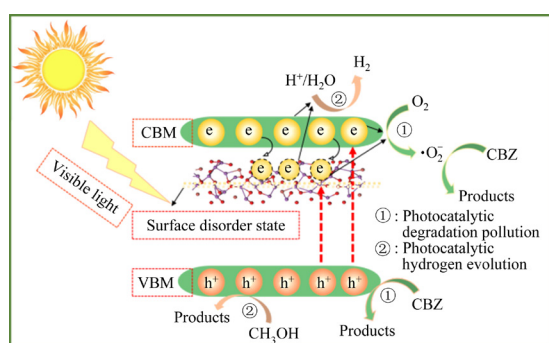
Fig. 7 Photocatalytic TC degradation and hydrogen evolution mechanism of O/D-Bi_5O_7Br

4 Conclusions

(1) Bi_5O_7Br with abundant ordered/disordered structures (O/D-Bi_5O_7Br) was in situ synthesized by a facile disorder engineering.

(2) Compared with the ordered Bi_5O_7Br (O-Bi_5O_7Br) and disordered Bi_5O_7Br (D-Bi_5O_7Br), Bi_5O_7Br with abundant ordered/disordered structures (O/D-Bi_5O_7Br) shows superior photocatalytic activity and stability for TC degradation activity and hydrogen evolution.

(3) The enhanced photocatalytic activity of O/D-Bi_5O_7Br is attributed to the unique ordered/ disordered structures of material, which can not only enhance light absorption ability, promote the reduction ability of photogenerated electrons, but also provide abundant unsaturated atoms as active sites for the photocatalytic process. Furthermore, in situ generation mode supplies barrier-free tight contact and accelerates charge transfer efficiently.

Acknowledgments

References

[1] SU Xin, LIU Can-jun, LIU Yang, YANG Ya-hui, LIU Xuan, CHEN Shu. Construction of $BiVO_4$ nanosheets@WO_3 arrays heterojunction photoanodes by versatile phase transformation strategy [J]. Transactions of Nonferrous Metals Society of China, 2021, 31: 533−544.

[2] LI Xiao-jing, WANG Jun-feng, ZHANG Jia-yu, ZHAO Chun-ran, WU Ying, HE Yi-ming. Cadmium sulfide modified zinc oxide heterojunction harvesting ultrasonic mechanical energy for efficient decomposition of dye wastewater [J]. Journal of Colloid and Interface Science, 2022, 607: 412−422.

[3] LI Yi, CHEN Hua-feng, WANG Lin-kun, WU Tian-tian, WU Ying, HE Yi-ming. $KNbO_3$/ZnO heterojunction harvesting ultrasonic mechanical energy and solar energy to efficiently degrade methyl orange [J]. Ultrasonics Sonochemistry, 2021, 78: 105754.

[4] YANG Yang, LAI Min, HUANG Jia-lei, LI Jin-ze, GAO Rui-jie, ZHAO Zi-ming, SONG Hua-tang, HE Ji-xiang, MA Yan. Bi_5O_7I/g-C_3N_4 heterostructures with enhanced visible-light photocatalytic performance for degradation of tetracycline hydrochloride [J]. Frontiers in Chemistry, 2021, 9: 781991.

[5] DONG Jin-tao, CHEN Feng, XU Li, YAN Peng-cheng, QIAN Jun-chao, CHEN Yun, YANG Meng-ying, LI He-nan. Fabrication of sensitive photoelectrochemical aptasensor using Ag nanoparticles sensitized bismuth oxyiodide for determination of chloramphenicol [J]. Microchemical Journal, 2022, 178: 107317.

[6] LI Rui, FENG Jun-qiang, ZHANG Xiao-chao, XIE Fang-xia, LIU Jian-xin, ZHANG Chang-ming, WANG Ya-wen, YUE Xiu-ping, FAN Cai-mei. In situ reorganization of Bi_3O_4Br nanosheet on the $Bi_{24}O_{31}Br_{10}$ ribbon structure for superior visible-light photocatalytic capability [J]. Separation and Purification Technology, 2020, 247: 117007.

[7] XIONG Hou-feng, ZOU Dong-lei, ZHOU Dan-dan, DONG Shuang-shi, WANG Jian-wei, RITTMANN B E. Enhancing degradation and mineralization of tetracycline using intimately coupled photocatalysis and biodegradation (ICPB) [J]. Chemical Engineering Journal, 2017, 316: 7−14.

[8] CHEN Peng-fei, CHEN Lu, GE Shi-feng, ZHANG Wen-qian, WU Meng-fei, XING Ping-xing, ROTAMOND T B, LIN Hong-jun, WU Ying, HE Yi-ming. Microwave heating preparation of phosphorus doped g-C_3N_4 and its enhanced performance for photocatalytic H_2 evolution in the help of Ag_3PO_4 nanoparticles [J]. International Journal of Hydrogen Energy, 2020, 45: 14354−14367.

[9] ZHANG Qing-le, CHEN Peng-fei, CHEN Lu, WU Meng-fei, DAI Xiao-quan, XING Ping-xing, LIN Hong-jun, ZHAO Lei-hong, HE Yi-ming. Facile fabrication of novel Ag_2S/K-g-C_3N_4 composite and its enhanced performance in

photocatalytic H_2 evolution [J]. Journal of Colloid and Interface Science, 2020, 568: 117−129.

[10] ZHAO Jun-ze, JI Meng-xia, CHEN Hai-long, WENG Yu-xiang, ZHONG Jun, LI Ying-jie, WANG Sheng-yao, CHEN Zi-ran, XIA Jie-xiang, LI Hua-ming. Interfacial chemical bond modulated $Bi_{19}S_{27}Br_3$/g-C_3N_4 Z-scheme heterojunction for enhanced photocatalytic CO_2 conversion [J]. Applied Catalysis B: Environmental, 2022, 307: 121162.

[11] PENG Yang, CHEN Jia, JIANG Liang-xing, WANG Tian-yi, YANG Hai-chao, LIU Fang-yang, JIA Ming. Preparation of Sb_2O_3/Sb_2S_3/FeOOH composite photoanodes for enhanced photoelectrochemical water oxidation [J]. Transactions of Nonferrous Metals Society of China, 2020, 30: 1625−1634.

[12] ZHANG Lu-lu, YUE Xiu-ping, LIU Jian-xin, FENG Jun-qiang, ZHANG Xiao-chao, ZHANG Chang-ming, LI Rui, FAN Cai-mei. Facile synthesis of Bi_5O_7Br/BiOBr 2D/3D heterojunction as efficient visible-light-driven photocatalyst for pharmaceutical organic degradation [J]. Separation and Purification Technology, 2020, 231: 115917.

[13] FU Si-mei, LI Gang-sen, WEN Xing, FAN Cai-mei, LIU Jian-xin, ZHANG Xiao-chao, LI Rui. Effect of calcination temperature on microstructure and photocatalytic activity of BiOX (X=Cl, Br) [J]. Transactions of Nonferrous Metals Society of China, 2020, 30: 765−773.

[14] CAI Zheng-qing, HUANG Yi-ning, JI Hao-dong, LIU Wen, FU Jie, SUN Xian-bo. Type-II surface heterojunction of bismuth-rich $Bi_4O_5Br_2$ on nitrogen-rich g-C_3N_5 nanosheets for efficient photocatalytic degradation of antibiotics [J]. Separation and Purification Technology, 2021, 280: 119772.

[15] LONG Ze-qing, XIAN Guang, ZHANG Guang-ming, ZHANG Tao, LI Xue-mei. BiOCl−$Bi_{12}O_{17}Cl_2$ nanocomposite with high visible-light photocatalytic activity prepared by an ultrasonic hydrothermal method for removing dye and pharmaceutical [J]. Chinese Journal of Catalysis, 2020, 41(3): 464−473.

[16] JIN Xiao-li, YE Li-qun, XIE Hai-quan, CHEN Gang. Bismuth-rich bismuth oxyhalides for environmental and energy photocatalysis [J]. Coordination Chemistry Reviews, 2017, 349: 84−101.

[17] KANG Yu-yang, YANG Yong-qiang, YIN Li-chang, KANG Xian-dong, LIU Gang, CHENG Hui-ming. An amorphous carbon nitride photocatalyst with greatly extended visible-light-responsive range for photocatalytic hydrogen generation [J]. Advanced Materials, 2015, 27: 4572−4577.

[18] JIN Zhi-liang, JIAN Qi-yan, GAO Qing-jie. Enhanced photocatalytic hydrogen evolution over semi-crystalline tungsten phosphide [J]. International Journal of Hydrogen Energy, 2019, 44: 26848−26862.

[19] RADHA R, RAVI KUMAR Y, SAKAR M, ROHITH VINOD K, BALAKUMAI S. Understanding the lattice composition directed in situ structural disorder for enhanced visible light photocatalytic activity in Bismuth iron niobate pyrochlore [J]. Applied Catalysis B: Environmental, 2018, 225: 386−396.

[20] WANG Rui-min, FAN Hong-jun. The mechanism of H_2 and H_2O desorption from bridging hydroxyls of a TiO_2 (110) surface [J]. Catalysis Science & Technology, 2017, 7: 251−264.

[21] YAN Xiao-dong, TIAN Li-hong, HE Min, CHEN Xiao-bo. Three-dimensional crystalline/amorphous Co/Co_3O_4 core/shell nanosheets as efficient electrocatalysts for the hydrogen evolution reaction [J]. Nano Letters, 2015, 15: 6015−6021.

[22] LV Cha-de, YAN Chun-shuang, CHEN Gang, DING Yu, SUN Jing-xue, ZHOU Yan-song, YU Gui-hua. An amorphous noble-metal-free electrocatalyst that enables nitrogen fixation under ambient conditions [J]. Angewandte Chemie International Edition, 2018, 57: 6073−6076.

[23] FENG Xiang-wen, CHEN Huan, JIANG Fang, WANG Xin. Enhanced visible-light photocatalytic nitrogen fixation over semicrystalline graphitic carbon nitride: Oxygen and sulfur co-doping for crystal and electronic structure modulation [J]. Journal of Colloid and Interface Science, 2018, 509: 298−306.

[24] WU Qing-ping, CHENG Yao, HUANG Feng, LI Xiao, CUI Xiang-shui, XU Ju, WANG Yuan-sheng. In-situ creating elastic lattice O—O bonds over semicrystalline yellow TiO_2 nanoparticles for significantly enhanced photocatalytic H_2 production [J]. Journal of Hazardous Materials, 2019, 374: 287−295.

[25] YU Zong-bao, YIN Li-chang, XIE Ying-peng, LIU Gang, MA Xiu-liang, CHENG Hui-ming. Crystallinity-dependent substitutional nitrogen doping in ZnO and its improved visible light photocatalytic activity [J]. Journal of Colloid and Interface Science, 2013, 400: 18−23.

[26] XIE Jun-feng, ZHANG Jia-jia, LI Shuang, GROTE F, ZHANG Xiao-dong, ZHANG Hao, WANG Ruo-xing, LEI Yong, PAN Bi-cai, XIE Yi. Controllable disorder engineering in oxygen-incorporated MoS_2 ultrathin nanosheets for efficient hydrogen evolution [J]. Journal of the American Chemical Society, 2013, 135: 17881−17888.

[27] WANG Hui, SUN Xian-shun, LI Dan-dan, ZHANG Xiao-dong, CHEN Shi-chuan, SHAO Wei, TIAN Yu-peng, XIE Yi. Boosting hot-electron generation: exciton dissociation at the order−disorder interfaces in polymeric photocatalysts [J]. Journal of the American Chemical Society, 2017, 139: 2468−2473.

[28] LIU Gao-peng, WANG Bin, ZHU Xing-wang, DING Peng-hui, ZHAO Jun-ze, LI Hua-ming, CHEN Zi-ran, ZHU Wen-shuai, XIA Jie-xiang. Edge-site-rich ordered macroporous BiOCl triggers C=O activation for efficient CO_2 photoreduction [J]. Small, 2022, 18: 2105228.

[29] XIONG Xu-yang, ZHOU Teng-fei, LIU Xiu-fan, DING Shuo-ping, HU Jun-cheng. Surfactant-mediated synthesis of single-crystalline Bi_3O_4Br nanorings with enhanced photocatalytic activity [J]. Journal of Materials Chemistry A, 2017, 5: 15706−15713.

[30] XUE Xiao-lan, CHEN Ren-peng, CHEN Hong-wei, HU Yi, DING Qing-qing, LIU Zi-teng, MA Lian-bo, ZHU Guo-yin, ZHANG Wen-jun, YU Qian, LIU Jie, MA Jing, JIN Zhong. Oxygen vacancy engineering promoted photocatalytic ammonia synthesis on ultrathin two-dimensional bismuth oxybromide nanosheets [J]. Nano Letters, 2018, 18: 7372−7377.

[31] HUO Yu-ning, ZHANG Jia, MIAO Miao, JIN Yi. Solvothermal synthesis of flower-like BiOBr microspheres with highly visible-light photocatalytic performances [J]. Applied Catalysis B: Environmental, 2012, 111/112: 334−341.

[32] CAI Jin-meng, ZHU Ying-ming, LIU Dong-sheng, MENG Ming, HU Zhen-peng, JIANG Zheng. Synergistic effect of titanate-anatase heterostructure and hydrogenation-induced surface disorder on photocatalytic water splitting [J]. ACS Catalysis, 2015, 5: 1708−1716.

[33] ZHANG Yi, DI Jun, QIAN Xu, JI Meng-xia, TIAN Zi-qi, YE Li-qun, ZHAO Jun-ze, YIN Sheng, LI Hua-ming, XIA Jie-xiang. Oxygen vacancies in $Bi_2Sn_2O_7$ quantum dots to trigger efficient photocatalytic nitrogen reduction [J]. Applied Catalysis B: Environmental, 2021, 299: 120680.

[34] TIAN Tian, ZHENG Min, LIN Jun-qi, MENG Xiang-yu, DING Yong. Amorphous Ni−Fe double hydroxide hollow nanocubes enriched with oxygen vacancies as efficient electrocatalytic water oxidation catalysts [J]. Chemical Communications, 2019, 55: 1044−1047.

[35] CAI Jin-meng, WANG Ya-ting, ZHU Ying-ming, WU Mo-qing, ZHANG Hao, LI Xin-gang, JIANG Zheng, MENG Ming. In situ formation of disorder-engineered $TiO_2(B)$-anatase heterophase junction for enhanced photocatalytic hydrogen evolution [J]. ACS Applied Materials & Interfaces, 2015, 7: 24987−24992.

[36] QIAN Kai-cheng, DU Lei-lei, ZHU Xiao-hui, LIANG Shi-pan, CHEN Shuang, KOBAYASHI H, YAN Xiao-qing, XU Min, DAI Yi-hu, LI Ren-hong. Directional oxygen activation by oxygen-vacancy-rich WO_2 nanorods for superb hydrogen evolution via formaldehyde reforming [J]. Journal of Materials Chemistry A, 2019, 7: 14592−14601.

[37] WANG Si-yuan, YANG Hua, WANG Xiang-xian, FENG Wang-jun. Surface disorder engineering of flake-like Bi_2WO_6 crystals for enhanced photocatalytic activity [J]. Journal of Electronic Materials, 2019, 48: 2067−2076.

[38] LI Jia-li, ZHAO Yu-xin, XIA Meng-yang, AN Hua, BAI Hong-cun, WEI Jin-jia, YANG Bo-lun, YANG Gui-dong. Highly efficient charge transfer at 2D/2D layered $P-La_2Ti_2O_7/Bi_2WO_6$ contact heterojunctions for upgraded visible-light-driven photocatalysis [J]. Applied Catalysis B: Environmental, 2020, 261: 118244.

[39] ZHANG Ying-guang, WU Mu-yan, KWOK Y H, WANG Yi-fei, ZHAO Wei, ZHAO Xiao-long, HUANG Hai-bao, LEUNG D Y C. In-situ synthesis of heterojunction TiO_2/MnO_2 nanostructure with excellent performance in vacuum ultraviolet photocatalytic oxidation of toluene [J]. Applied Catalysis B: Environmental, 2019, 259: 118034.

[40] WU Xue-lian, NG Y H, WANG Liang, DU Yi, DOU Shi-xue, AMAL R, SCOTT J. Improving the photo-oxidative capability of BiOBr via crystal facet engineering [J]. Journal of Materials Chemistry A, 2017, 5: 8117−8124.

[41] HAO Lin, HUANG Hong-wei, GUO Yu-xi, DU Xin, ZHANG Yi-he. Bismuth oxychloride homogeneous phase junction $BiOCl/Bi_{12}O_{17}Cl_2$ with unselectively efficient photocatalytic activity and mechanism insight [J]. Applied Surface Science, 2017, 420: 303−312.

[42] LI Rui, LIU Jian-xin, ZHANG Xing-fang, WANG Ya-wen, WANG Yun-fang, ZHANG Chang-ming, ZHANG Xiao-chao, FAN Cai-mei. Iodide-modified $Bi_4O_5Br_2$ photocatalyst with tunable conduction band position for efficient visible-light decontamination of pollutants [J]. Chemical Engineering Journal, 2018, 339: 42−50.

采用原位无序工程提高 Bi_5O_7Br 的 可见光光催化药物降解和析氢性能

谢芳霞 [1,2]，张璐璐 [2]，张 潇 [1]，张 媚 [2]，简 选 [3]，
刘建新 [2]，张小超 [2]，王雅文 [2]，李 瑞 [1,2]，樊彩梅 [1,2]

1. 太原理工大学 环境科学与工程学院，太原 030024；
2. 太原理工大学 化学工程与技术学院，太原 030024；
3. 延安大学 化学化工学院 陕西省化学反应工程重点实验室，延安 716000

摘 要：为了同时解决光吸收能力弱和光生载流子复合率高的问题，本文作者通过简单的原位无序工程合成具有丰富有序/无序结构的 Bi_5O_7Br (O/D-Bi_5O_7Br) 光催化剂。采用 XRD、TEM、HRTEM、SAED、XPS 和 UV-Vis DRS 对所制备的样品进行表征，并通过可见光催化降解盐酸四环素(TC)和光解水析氢评价其光催化活性。结果表明，有序/无序结构不仅增强了 Bi_5O_7Br 的光吸收能力，提高了其导带位置，促进了光生载流子的转移和分离，而且为光催化过程提供了丰富的不饱和原子作为反应活性位点。因此，O/D-Bi_5O_7Br 表现出 38.12 μmol/(g·h)的高析氢率和在 135 min 内 86%的 TC 降解率。

关键词：Bi_5O_7Br；无序工程；药物降解；析氢；可见光

(Edited by Wei-ping CHEN)